This article has been accepted for publication in a future issue of this journal, but has not been fully edited. Content may change prior to final publication. Citation information: DOI 10.1109/TAP.2019.2902639, IEEE Transactions on Antennas and Propagation

Radiation Properties of a 2D Periodic Leaky-Wave Antenna

Sohini Sengupta, David R. Jackson, Ahmad T. Almutawa, Hamidreza Kazemi, Filippo Capolino, and Stuart A. Long

***Abstract*—A study of the radiation characteristics of a two-dimensional (2D) periodic leaky-wave antenna (LWA) (i.e., one that radiates from *higher-order* space harmonics (Floquet waves) instead of the fundamental one) is presented here for the first time, and an optimization to produce maximum radiation at broadside is discussed. The structure consists of a 2D periodic arrangement of narrow rectangular patches on a grounded dielectric substrate, excited by a simple source such as a slot in the ground plane. A 2D periodic leaky-wave antenna can be designed to radiate a narrow pencil beam pattern at broadside by adjusting its geometric parameters. The main beam at broadside is narrower in the E plane than in the H plane, and there are also grating lobes introduced due to the periodicity. The structure has been analyzed theoretically using the periodic spectral domain immittance (periodic SDI) method. The proposed antenna has also been simulated using both FEM and MoM methods and a fabricated design has been measured. A good correlation is observed between the theoretical, simulated, and measured radiation patterns.**

***Index Terms*—2D periodic leaky-wave antenna, leaky-wave antenna, periodic leaky-wave antenna.**

I. Introduction

THE first leaky-wave antenna (LWA) was a waveguide with a slit along its side [1, 2], forming a 1D uniform LWA. Then came waveguides with closely spaced holes instead of a slit, forming a 1D quasi-uniform LWA, which produced narrower beams by having less perturbations per unit length [3]. In [4] the concept of introducing a uniform or periodic asymmetry to turn a waveguide or transmission line structure into a leaky-wave antenna was first introduced. Oliner and others did a lot of work on 1D LWAs, and a comprehensive report was published in [5]. Von Trentini introduced the concept of the Fabry-Pérot resonant cavity antenna (FPRCA) that employed a 2D periodic partially reflective surface (PRS) over a ground plane in order to produce narrow pencil beams at broadside [6]. This structure was actually the first quasi-uniform 2D LWA, although it was not recognized at first as such. Jackson and Alexopoulos studied uniform 2D LWAs consisting of a superstrate over a grounded substrate in [7, 8], though again it was not originally recognized that this structure was acting as a 2D LWA. This structure was further analyzed by Jackson and Oliner in [9, 10] from a leaky-wave point of view. A 2D LWA using a PRS was further explored in [11] using different kinds of elements. The radiation characteristics of a 2D quasi-uniform LWA with metal patches and slots was studied in [11, 12].

More recently, metamaterial structures have also been used in the design of 1D and 2D LWAs [13–16]. Substrate integrated waveguide (SIW) leaky-wave antennas have also been studied, for example in [17] where a 1D slotted SIW leaky-wave antenna that has frequency-dependent beam scanning from near broadside to forward end-fire is examined. Another design for a 1D SIW LWA uses leakage from the periodic via walls to create a LWA [18].

The design of a leaky-wave antenna with a double-strip grating was proposed in [19], which consists of two strips per unit cell. With this design the stopband behavior around the broadside scan region can almost be eliminated. The radiation patterns from a 2D Electromagnetic Band Gap (EBG) structure were studied in [20]. The structure consists of a metallic strip grating over a grounded dielectric substrate excited by a line source. In [21–23] methods for understanding and analyzing 1D and 2D LWAs from a fundamental perspective was given. In [24] an array factor approach was proposed for fast and efficient computation of the radiation pattern of complex 1D and 2D metamaterial leaky-wave structures of arbitrary size.

A LWA consisting of a metallic grating of concentric annular rings fed by a non-directive TM_0 surface wave source was presented in [25]. To ensure only the leakage of the TM_0 field and its radiation into the far-field region, the launching of a TE polarized field distribution was suppressed over a large bandwidth. The design of a conformal leaky-wave antenna (CLWA) with a metal strip grating on a curved surface that utilizes a backward-radiating leaky wave to focus the beam

S. Sengupta was previously with the Department of Electrical and Computer Engineering, and the Department of Mathematics, University of Houston, Houston, TX 77204 USA. She is presently with the Energous Corporation, San Jose, CA 95134 USA (e-mail: sohiniseng@gmail.com).

D. R. Jackson is with the Department of Electrical and Computer Engineering, University of Houston, Houston, TX 77204-4005 USA (e-mail: djackson@uh.edu).

A. T. Almutawa is with the Department of Electrical Engineering and Computer Science, University of California, Irvine, Irvine, CA 92697-2625 USA, (e-mail: ahmed.almutawa@gmail.com).

H. Kazemi is with the Department of Electrical Engineering and Computer Science, University of California, Irvine, Irvine, CA 92697-2625 USA, (e-mail: hamidrkazemi87@gmail.com).

F. Capolino is with the Department of Electrical Engineering and Computer Science, University of California, Irvine, Irvine, CA 92697-2625 USA, (e-mail: f.capolino@uci.edu).

S. A. Long is with the Department of Electrical and Computer Engineering, University of Houston, Houston, TX 77204-4005 USA, (e-mail: long@uh.edu).

This article has been accepted for publication in a future issue of this journal, but has not been fully edited. Content may change prior to final publication. Citation information: DOI 10.1109/TAP.2019.2902639, IEEE Transactions on Antennas and Propagation

was presented in [26].

There have been several studies done on the Fabry-Pérot resonant cavity antenna, which has a partially reflective surface (PRS) over a grounded dielectric slab [27, 28]. This class of antenna has a structure that is somewhat similar to the periodic leaky-wave antenna discussed in this paper, and some of the fundamental physics is the same; but it has a very different mode of operation. Some of these Fabry-Pérot antennas have an artificial magnetic conductor (AMC) as the ground plane instead of the usual electric conductor as the ground plane [29, 30]. This serves to reduce the height of the antenna structure. A simple way to solve for the complex wavenumber and therefore the dispersive characteristics of a thin periodic 2D Fabry-Pérot LWA was presented in [31].

The motivation for the present structure (2D periodic LWA) comes from the phenomena of directive beaming of light through a sub-wavelength aperture in a plasmonic structure at optical frequencies [32, 33], which was shown to be produced by leaky-plasmon-waves in [34, 35]. The 2D leaky-wave antenna studied here is shown in Fig. 1. This particular structure has been explored from the perspective of propagation of leaky-wave modes in the structure in [36, 37], and was also discussed briefly in [38, 39]. It consists of a grounded dielectric slab with an array of rectangular patches on the upper surface distributed periodically in a rectangular lattice. This structure is excited here by a slot in the ground plane. The length and width of the patches are given by L and W, and the period of the unit cell in the x and y directions are given by a and b, respectively. The structure can be infinite in the x and y directions, or truncated to create a finite radiating aperture, for practical fabrication.

Throughout the study here, the frequency is chosen to be f = 12 GHz. The substrate has a relative permittivity of ε_r = 9.8, a loss tangent of $\tan\delta$ = 0.002, and the height of substrate is h = 1.27 mm. (For some of the calculations, the substrate is assumed to be lossless, however.) The excitation is provided by a narrow y-directed slot in the ground plane that is modeled as an infinitesimal magnetic dipole. The origin is at the center (0,0) of the patch while the slot is centered between the patches at ($x_0 = -a/2$, $y_0 = 0$). The slot that excites the structure should ideally be placed along the line $x_0 = -a/2$, i.e., located halfway horizontally between adjacent columns of patches, to help maximize the minimum distance between the slot and the surrounding patches. If the slot is placed close to a particular patch, e.g., directly below the center of a patch ($x_0 = 0$, $y_0 = 0$), there will be strong coupling between the slot and that patch, which will set up a strong current on that patch. That patch will then radiate strongly, essentially acting as a slot-fed microstrip patch antenna. That will result in undesirable secondary radiation, since the objective here is to have radiation coming from the leaky mode alone. Results (omitted) show that when the slot is placed directly below the center of a patch, the pattern is degraded, with an increased level of "space-wave" radiation (radiation that comes directly from the feed region, as opposed to coming from the leaky mode that is spread out over the entire radiating aperture). The choice ($x_0 = -a/2$, $y_0 = 0$) is adopted here for all of the results.

The height of the substrate is chosen such that only a TM_0 surface wave is excited within the grounded dielectric slab by the slot; therefore

$$h < \frac{\lambda_0/4}{\sqrt{\varepsilon_r - 1}}, \tag{1}$$

where λ_0 is the wavelength in free space.

The TM_0 surface wave is the mode that becomes a leaky mode, due to the periodic metal patches, and the radiation from the higher-order space harmonics of the TM_0 surface-wave mode, which is now a leaky mode, does the beam forming. The magnetic dipole in the y direction launches the TM_0 surface wave with a $\cos\phi$ pattern, so the E plane (ϕ = 0) is expected to be more influenced by this leaky mode than the H plane ($\phi = \pi/2$). A more complete discussion of the leaky-mode propagation characteristics for this structure may be found in [36], including a discussion of how the wavenumbers of the leaky mode are very different in the E plane and the H plane (which results in very different beamwidths in these two planes). In the present work, the focus is on the radiation and antenna properties of this structure, including the main beam and the grating lobes.

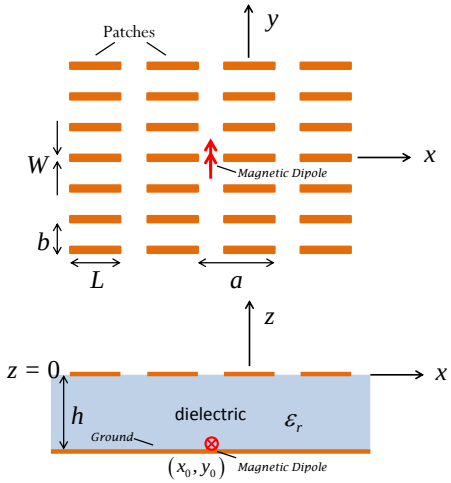

Fig. 1. Schematic of the 2D periodic leaky-wave antenna with the slot in the ground plane modeled as a magnetic dipole.

II. Far Field Pattern

Since the 2D periodic leaky-wave antenna structure consists of a layered media with periodic metallization on the surface, the structure can be theoretically analyzed using the method of moments together with the periodic spectral domain immittance method.

Figure 2 shows a side-view of a portion of the 2D periodic LWA structure, with the grounded dielectric slab and metal patches on the upper surface. The magnetic dipole source is located at (x_0, y_0, $-h_d$), with $h_d = h$ here since the magnetic dipole models a slot in the ground plane. The magnetic dipole source is taken to be unit amplitude (Kl = 1Vm) for simplicity. A "testing" dipole is also shown here located at (r, θ, ϕ), where $r \to \infty$ for the purpose of calculating the radiation pattern in the far-field region using reciprocity [12].

This article has been accepted for publication in a future issue of this journal, but has not been fully edited. Content may change prior to final publication. Citation information: DOI 10.1109/TAP.2019.2902639, IEEE Transactions on Antennas and Propagation

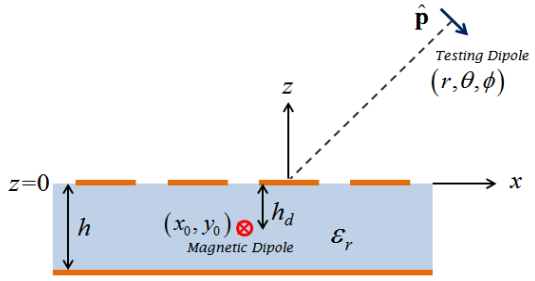

Fig. 2. Side view of the 2D periodic leaky-wave antenna, showing the testing dipole that is used for the far-field calculation.

The testing dipole is an infinitesimal electric dipole located in the direction of unit vector $\hat{\mathbf{p}}$, which is chosen as $\hat{\boldsymbol{\theta}}$ for calculating E_θ and $\hat{\boldsymbol{\phi}}$ for calculating E_ϕ. The incident field from the testing dipole is a plane wave that is polarized as TM_z (TE_z) for $\hat{\mathbf{p}} = \hat{\boldsymbol{\theta}}$ ($\hat{\boldsymbol{\phi}}$), and is given by

$$\mathbf{E}^{\text{inc}}(x,y,z) = \hat{\mathbf{p}}\left(-\frac{j\omega\mu}{4\pi r}e^{-jk_0 r}\right)e^{-j\mathbf{k}\cdot\mathbf{r}}. \tag{2}$$

Here r is the distance of the testing dipole from the origin, $\mathbf{r}$ is the vector location of an arbitrary point (x, y, z) near the structure, and the incident wavenumber of the plane wave is

$$\mathbf{k} = k_x^{\text{PW}}\hat{\mathbf{x}} + k_y^{\text{PW}}\hat{\mathbf{y}} + k_z^{\text{PW}}\hat{\mathbf{z}}, \tag{3}$$

where $k_x^{\text{PW}} = -k_0\sin\theta\cos\phi = k_{x0}$, $k_y^{\text{PW}} = -k_0\sin\theta\sin\phi = k_{y0}$, and $k_z^{\text{PW}} = -k_0\cos\theta = -k_{z0}$.

The total E field on the surface of the patches is given by

$$\mathbf{E}^{\text{total}} = \mathbf{E}^{\text{layer}} + \mathbf{E}^{\text{sca}}, \tag{4}$$

where the "layer" field, $\mathbf{E}^{\text{layer}}$, is that produced in the absence of the patches (i.e., by the layered structure only), and the scattered field $\mathbf{E}^{\text{sca}}$ is that due to the radiating currents of the patches.

Considering the field in the x-direction,

$$E_x^{\text{layer}} = E_x^{\text{inc}}(1+\Gamma), \text{ where } \Gamma = \frac{jZ_1\tan(k_{z1}h) - Z_0}{jZ_1\tan(k_{z1}h) + Z_0}. \tag{5}$$

The incident field from the testing dipole is reflected from the grounded slab and also scattered by the patches. The scattered field is given by

$$E_x^{\text{sca}} = \frac{1}{ab}\sum_{p=-\infty}^{\infty}\sum_{q=-\infty}^{\infty}\tilde{G}_{xx}^{EJ}(k_{xp},k_{yq})\tilde{J}_{sx}^{p}(k_{xp},k_{yq})e^{-j(k_{xp}x+k_{yq}y)}, \tag{6}$$

where

$$\begin{aligned}\tilde{G}_{xx}^{EJ}(k_x,k_y) &= -\frac{1}{k_t^2}\left[k_x^2 V_i^{TM} + k_y^2 V_i^{TE}\right] \\ &= -\frac{1}{k_t^2}\left[\frac{k_x^2}{D_{TM}(k_x,k_y)} + \frac{k_y^2}{D_{TE}(k_x,k_y)}\right],\end{aligned} \tag{7}$$

where

$$D_{TM}(k_x,k_y) = Y_0^{TM} - jY_1^{TM}\cot(k_{z1}h) \tag{8}$$

and

$$D_{TE}(k_x,k_y) = Y_0^{TE} - jY_1^{TE}\cot(k_{z1}h). \tag{9}$$

The derivation of the Green's function $\tilde{G}_{xx}^{EJ}(k_x,k_y)$ is done using the spectral domain immittance method, together with the Transverse Equivalent Network (TEN) method, which models the layers as sections of transmission lines and models the variation of the fields in the z direction [36]. The derivation is omitted here for brevity. The voltages $V_i^{TM}(z)$ and $V_i^{TE}(z)$ are the voltages on the TEN due to a 1A parallel current source, as shown in Fig. 3 [40].

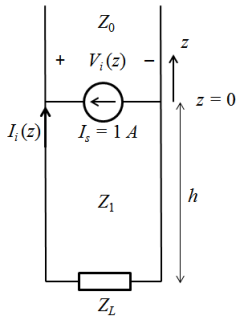

Fig. 3. TEN model for the 2D periodic LWA structure with the patch currents as the source.

In Fig. 3, Z_0 and Z_1 are the characteristic impedances within the air and the dielectric medium respectively, and $Z_L = 0$ if we assume a PEC ground plane as is done here (otherwise, a surface impedance can be used to model the ground plane). Here $h_d = h$, since the magnetic dipole source is on the ground plane.

Since the patches are very narrow in the y-direction and longer in the x-direction, the current on the patches is assumed to be in the x-direction only and is given by

$$J_{sx}^{p}(x,y) = \sum_{n=1}^{N} a_n B_n(x,y) = \sum_{n=1}^{N} a_n f_n(x) g_n(y), \tag{10}$$

where a_n is the coefficient of the n^{th} basis function $B_n(x,y)$ and

$$f_n(x) = \sin\left[\frac{n\pi}{L}\left(x+\frac{L}{2}\right)\right], \quad g_n(y) = \frac{1/\pi}{\sqrt{(W/2)^2 - y^2}}. \tag{11}$$

The Fourier transform of the patch current is then given by

$$\tilde{J}_{sx}^{p}(k_x,k_y) = \sum_{n=1}^{N} a_n \tilde{B}_n(k_x,k_y) = \sum_{n=1}^{N} a_n \tilde{f}_n(k_x)\tilde{g}_n(k_y), \tag{12}$$

where

$$\tilde{f}_n(k_x) = \frac{e^{-jk_x L/2}\left(-n\pi L + e^{jk_x L}L(n\pi\cos(n\pi))\right)}{(k_x L)^2 - (n\pi)^2} \tag{13}$$

and

$$\tilde{g}_n(k_y) = J_0(k_y W/2). \tag{14}$$

The method of moments [41], [42] is then applied by enforcing the electric field integral equation (EFIE) on the (0, 0)$^{\text{th}}$ patch (assuming it to be a perfect electric conductor) at z = 0 in the x-direction,

$$E_x^{\text{tot}} = E_x^{\text{layer}} + E_x^{\text{sca}} = 0. \tag{15}$$

Substituting from Eqs. (5) and (6), we have

$$E_x^{\text{inc}}(1+\Gamma) + \frac{1}{ab}\sum_{p=-\infty}^{\infty}\sum_{q=-\infty}^{\infty}\tilde{G}_{xx}^{EJ}(k_{xp},k_{yq})\tilde{J}_{sx}^{p}(k_{xp},k_{yq})e^{-j(k_{xp}x+k_{yq}y)} = 0. \tag{16}$$

Applying Galerkin's method and taking the testing function to have the same form as the basis function, we have

This article has been accepted for publication in a future issue of this journal, but has not been fully edited. Content may change prior to final publication. Citation information: DOI 10.1109/TAP.2019.2902639, IEEE Transactions on Antennas and Propagation

$$\int_{-w/2}^{w/2}\int_{-L/2}^{L/2}\frac{1}{ab}\sum_{p=-\infty}^{\infty}\sum_{q=-\infty}^{\infty}\tilde{G}_{xx}^{EJ}\left(k_{xp},k_{yq}\right)\tilde{J}_{sx}^{P}\left(k_{xp},k_{yq}\right)B_m\left(x,y\right)e^{-j\left(k_{xp}x+k_{yq}y\right)}dxdy$$
$$=-\int_{-w/2}^{w/2}\int_{-L/2}^{L/2}E_x^{\text{inc}}\left(x,y,0\right)\left(1+\Gamma\right)B_m\left(x,y\right)dxdy. \tag{17}$$

Replacing $\tilde{J}_{sx}^{P}\left(k_{xp},k_{yq}\right)$ from Eq. (12) and $E_x^{inc}\left(x,y,0\right)$ from Eq. (2) above, we have

$$\int_{-\frac{w}{2}}^{\frac{w}{2}}\int_{-\frac{L}{2}}^{\frac{L}{2}}\frac{1}{ab}\sum_{p=-\infty}^{\infty}\sum_{q=-\infty}^{\infty}\tilde{G}_{xx}^{EJ}\left(k_{xp},k_{yq}\right)\sum_{n=1}^{N}a_n\tilde{B}_n\left(k_{xp},k_{yq}\right)B_m\left(x,y\right)e^{-j\left(k_{xp}x+k_{yq}y\right)}dxdy$$
$$=-\int_{-w/2}^{w/2}\int_{-L/2}^{L/2}E_x^{\text{inc}}\left(0,0,0\right)e^{-j\left(k_{x0}x+k_{y0}y\right)}\left(1+\Gamma\right)B_m\left(x,y\right)dxdy \tag{18}$$

or

$$\sum_{n=1}^{N}a_n\frac{1}{ab}\sum_{p=-\infty}^{\infty}\sum_{q=-\infty}^{\infty}\tilde{G}_{xx}^{EJ}\left(k_{xp},k_{yq}\right)\tilde{B}_n\left(k_{xp},k_{yq}\right)\tilde{B}_m\left(-k_{xp},-k_{yq}\right)$$
$$=-E_x^{\text{inc}}\left(0,0,0\right)\left(1+\Gamma\right)\tilde{B}_m\left(-k_{x0},-k_{y0}\right). \tag{19}$$

The matrix form of the above EFIE relation is

$$\left[Z_{mn}\right]\left[a_n\right]=\left[R_m\right], \tag{20}$$

where

$$Z_{mn}=\frac{1}{ab}\sum_{p=-\infty}^{\infty}\sum_{q=-\infty}^{\infty}\tilde{G}_{xx}^{EJ}\left(k_{xp},k_{yq}\right)\tilde{B}_n\left(k_{xp},k_{yq}\right)\tilde{B}_m\left(-k_{xp},-k_{yq}\right)e^{-jk_{zpq0}\Delta z}. \tag{21}$$

Here Δz denotes the z-displacement between the current on the patches and the testing function, and

$$R_m=-E_x^{\text{inc}}\left(0,0,0\right)\left(1+\Gamma\right)\tilde{B}_m\left(-k_{x0},-k_{y0}\right). \tag{22}$$

The z-displacement Δz is added for easier convergence of the infinite summations in p and q and makes the computations easier. Practically, it can be thought of as accounting for an equivalent thickness of the conductor patches. Unless otherwise specified, the z-displacement has been applied in all numerically generated theoretical results presented in later sections, and it is taken to be $\Delta z = 0.01a$. As long as Δz is small, the results are almost independent of this value, so this is a convenient tool for accelerating the convergence. More sophisticated acceleration schemes could be used, but this simple scheme is reasonably effective. The above EFIE matrix equation is then solved for the coefficients of the basis function, a_n. Using reciprocity, the electric field in the far-field region is then calculated from the field H_y at the magnetic dipole location as

$$E_i^{\text{FF}}\left(r,\theta,\phi\right)=-H_y\left(x_0,y_0,-h_d\right)=-H_y\left(-a/2,0,-h_d\right). \tag{23}$$

The field H_y is due to the scattered field of the patches and the incident field impinging on the grounded slab, so that

$$E_i^{\text{FF}}\left(r,\theta,\phi\right)=\frac{1}{ab}\sum_{n=1}^{N}a_n\sum_{p=-\infty}^{\infty}\sum_{q=-\infty}^{\infty}\tilde{G}_{yx}^{HJ}\left(k_{xp},k_{yq}\right)\tilde{B}_n\left(k_{xp},k_{yq}\right)e^{-j\left(k_{xp}x_0+k_{yq}y_0\right)}$$
$$+E_x^{\text{inc}}\left(-\frac{1}{Z_0}\right)\left(1-\Gamma\right)\left\{\frac{e^{-jk_{z1}^{pw}h_d}\left(1-\Gamma_L e^{-j2k_{z1}^{pw}\left(h-h_d\right)}\right)}{\left(1-\Gamma_L e^{-j2k_{z1}^{pw}h}\right)}\right\}e^{-j\left(k_{x0}x_0+k_{y0}y_0\right)}. \tag{24}$$

Here $x_0=-a/2$, $y_0=0$, and $i=\theta$ for TM_z, ϕ for TE_z polarization. The Green's function $\tilde{G}_{yx}^{HJ}\left(k_x, k_y\right)$ is given by

$$\tilde{G}_{yx}^{HJ}\left(k_x,k_y\right)=-\frac{1}{k_t^2}\left[k_x^2I_i^{TM}\left(-h_d\right)+k_y^2I_i^{TE}\left(-h_d\right)\right]. \tag{25}$$

The currents $I_i^{TM}(z)$ and $I_i^{TE}(z)$ are the currents on the TEN due to a 1A parallel current source, as shown in Fig. 3. In this derivation we have used

$$I_i\left(-h_d\right)=I_i\left(0\right)\frac{e^{-jk_{z1}^{pw}h_d}\left(1-\Gamma_L e^{-j2k_{z1}^{pw}\left(h-h_d\right)}\right)}{\left(1-\Gamma_L e^{-j2k_{z1}^{pw}h}\right)},\quad \Gamma_L=\frac{Z_L-Z_1}{Z_L+Z_1} \tag{26}$$

to obtain the parenthetical term in Eq. (24). Since $Z_L = 0$, the reflection coefficient at the load Z_L is $\Gamma_L = -1$ and hence the above expression reduces to

$$I_i\left(-h_d\right)=I_i\left(0\right)\frac{\cos\left(k_{z1}^{pw}\left(h-h_d\right)\right)}{\cos\left(k_{z1}^{pw}h\right)}. \tag{27}$$

A more detailed derivation of the Green's functions can be found in [43].

III. Optimization

The 2D periodic leaky-wave antenna produces a three-dimensional conical main beam that can be optimized to converge into a narrow directive beam at broadside. The beam is optimized by adjusting the spatial period in the x-direction, a, to get the maximum power density radiated at broadside, keeping all other parameters fixed for a given length L and width W of the patches, including the substrate properties. The spatial period in the y-direction, b, is either kept fixed or is taken to be a constant fraction of a (such as $b = a/1.2$) in later results. First, however, Fig. 4 shows a contour plot of the far field broadside power density (in dB, relative to 1 W/m^2) for a range of values of both a and b (coming from Eq. (24)). For this case the substrate is taken to be lossless with $\tan\delta = 0$. The length of the patch is L = 0.25 cm and width is $W = L/5$. The far field is calculated using reciprocity and the periodic SDI method as described in section II.

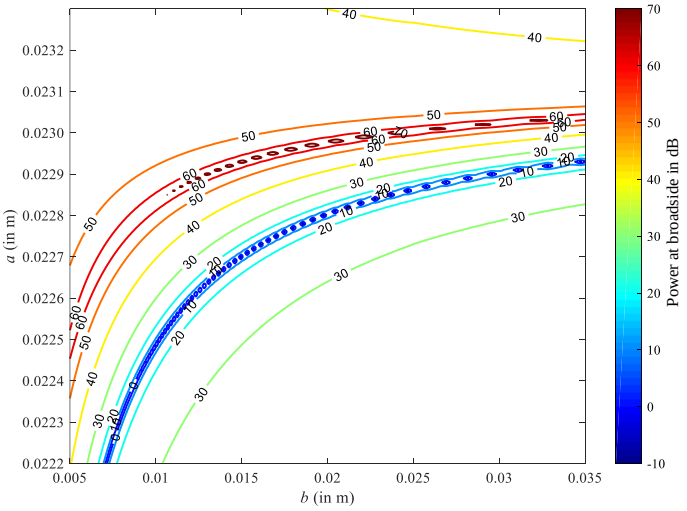

Fig. 4. Contour plot of the power density radiated at broadside for different values of a and b.

This article has been accepted for publication in a future issue of this journal, but has not been fully edited. Content may change prior to final publication. Citation information: DOI 10.1109/TAP.2019.2902639, IEEE Transactions on Antennas and Propagation

In Fig. 4, the band of red (in the color version) is the region of highest power density and the plot shows that this region is shaped somewhat like a ridge that spans the entire range of values for b; there is no clear maxima seen on this color scale within the ridge. This means that for a large range of values for b, one can choose a value of a to get nearly optimum power density radiated at broadside. The optimum value of a will depend on the value of b, although the dependence is not very great, since the ridge is fairly flat through most of the range. The optimum value of a corresponds to roughly 0.23 cm, slightly less than one free-space wavelength (λ_0 = 0.25 cm at 12 GHz). This is not a coincidence. In the E plane, the radiating space harmonic (Floquet wave) is the (−1,0) harmonic of the leaky mode. If we assume that the metal patches do not disturb the phase constant β_{TM0} of the surface wave too much, then the phase constant of the (−1,0) harmonic of the leaky mode propagating in the E plane direction (in the x direction) will be given approximately by

$$\beta_{-1,0} \approx \beta_{TM_0} - \frac{2\pi}{a}. \tag{28}$$

If the substrate is not too thick (typically $h < 0.05\ \lambda_0$), then β_{TM0} will be close to k_0. (For example, for the substrate in Fig. 4, where $h = 0.051\lambda_0$, $\beta_{\mathrm{TM0}} = 1.08\ k_0$.) If we make this assumption and set $\beta_{-1,0} = 0$ corresponding to broadside radiation, we obtain $a = \lambda_0$.

Figure 5 shows the magnitude of the E field at broadside (from Eq. (24)) plotted with respect to b, when the power density at broadside has been maximized by adjusting a for each given value of b (we are operating at the peak of the red ridge in Fig. 4).

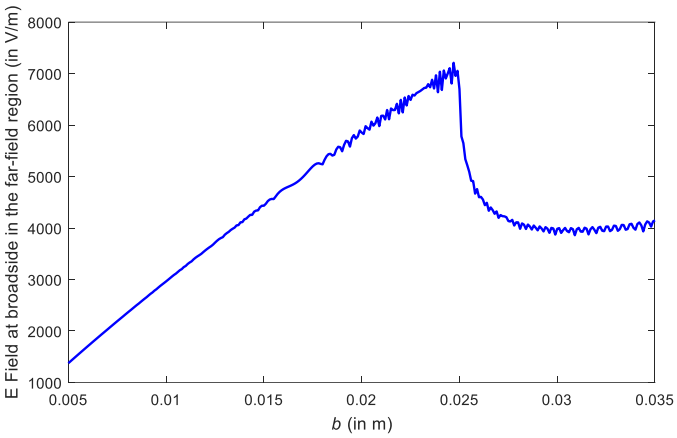

Fig. 5. Optimized maximum electric field magnitude at broadside vs. b.

Figure 5 shows that there is a value of b (0.025 m, corresponding to $b = \lambda_0$) that gives the maximum power radiation at broadside; but this might not be considered a good design as there will be many grating lobes in the radiation pattern when b is this large. It has been observed that choosing a lower value of b reduces the grating lobes in the radiation pattern. So, there is a trade-off in the design between power density radiated at broadside and grating lobes. Choosing $b = a/1.2$ gives roughly a 20% "safety margin".

IV. Radiation Patterns

Radiation patterns for a case with a small patch size are first shown here, which were calculated using the method described in section II. In the cases shown in Figs. 6 and 7 the frequency is 12 GHz, the length of the patches is L = 0.25 cm, the width is $W = L/5$, and the dimensions of the unit cell are given by a = 2.297 cm and $b = a/1.2$. Here the substrate is taken to be lossy with $\tan\delta$ = 0.002. In this case the enhancement factor is 78.7. The enhancement factor (EF) is defined here as the magnitude of the E field radiated at broadside, divided by the value radiated by the same magnetic dipole source in free space. This is a measure of how much the leaky-wave antenna structure enhances the power density of the radiation at broadside. It is also indirectly a measure of the directivity of the antenna (though not exactly proportional to it, since the total power radiated by the dipole will change when the antenna structure is present). Figure 6 shows the principal planes and the 45° diagonal plane (D plane), while Fig. 7 shows the pattern in other ϕ planes.

Perhaps the most obvious feature of the patterns in Fig. 6 is that the E plane pattern is much narrower (by roughly a factor of 10) than the H plane pattern. This is because the main beam at broadside is produced mainly by the (−1, 0) Floquet mode of the leaky mode along the E plane and the (0, −1) Floquet mode along the H plane. The wavenumber of the leaky mode that produces the radiation is very different in the E and H planes, however. In the E plane, the leaky mode is a perturbation of the TM_0 surface wave mode of the grounded slab, and the magnetic dipole launches this mode strongly in the E plane direction. However, the magnetic dipole launches the TM_0 surface wave much less strongly in the H plane direction. In fact, the simple $\cos\phi$ formula predicts no launching of the surface wave at all in the H plane direction ($\phi = \pi/2$). However, the $\cos\phi$ formula applies to the dominant components of the TM_0 surface wave, namely the E_z, H_ϕ, E_ρ components. Higher-order field components including E_ϕ and H_ρ are excited with a $\sin\phi$ variation. This causes the field structure of the leaky mode in the H plane to be different from that in the E plane; the field is polarized and configured differently from that in the E plane, and it does not resemble the field structure of the TM_0 surface wave [36]. As a consequence, the attenuation constant of the leaky mode in the H plane is very different, about 10 times larger, than that of the leaky mode in the E plane. This is why the beamwidths are different by about a factor of 10.

Another comment is that the E and H plane patterns are free from grating lobes, but the D plane is not. The D plane has a beamwidth that is very similar to that of the E plane (the two patterns are almost superimposed in the main beam region), with the main difference being the very narrow grating lobes seen in the D plane at about θ = 20° and 38°. The grating lobe phenomenon is due to radiation from various space harmonics arising from the leaky mode propagating at different angles ϕ on the structure [36].

Away from the main beam region, the E plane pattern has a level of space-wave radiation that is about −25 dB from the

This article has been accepted for publication in a future issue of this journal, but has not been fully edited. Content may change prior to final publication. Citation information: DOI 10.1109/TAP.2019.2902639, IEEE Transactions on Antennas and Propagation

main beam. This is mainly due to direct radiation from the source (magnetic dipole) that does not get channeled in the TM_0 surface wave. The space-wave pattern is very broad, as opposed to the main beam, which is due to focused radiation from the leaky mode (or more precisely, from the relevant space harmonic of the leaky mode). The main beam is narrow due to the small patch length (0.25 cm), which results in small attenuation constants of the leaky mode in the E and H planes.

Figure 7 makes it clear that for pattern cuts away from the principal planes, grating lobes appear. Three different cuts are shown (ϕ = 30º, 60º, 75º), and they all display narrow grating beams. Grating beams in the off-principal planes seem to be an unavoidable consequence of this type of 2D periodic LWA. This is because the structure radiates from space harmonics, as opposed to a Fabry-Pérot resonant cavity type of LWA, which radiates only from the fundamental (0, 0) space harmonic, even if the structure contains a PRS that is periodic. In both cases there is a radially-propagating leaky mode on the structure, emanating from the source. However, for the 2D periodic LWA, radiation from the (−1,0) and (0,−1) harmonics of the leaky mode in the E and H planes form the main beam. Unfortunately, these same harmonics (and also the (−1,−1) harmonic) result in grating beams when the leaky mode is propagating in other directions (off of the principal planes) on the structure. This seems unavoidable. However, the grating lobe problem is accentuated here because of the infinite structure, which allows for grating beams of very small beamwidths to be created. The beamwidth of a grating beam is determined by the attenuation constant of the radiating Floquet wave, determined by the attenuation constant vector of the leaky mode projected in the direction of the relevant ϕ cut. This attenuation constant can become very small, even much smaller than the attenuation constant of the leaky mode itself. A more detailed analysis of the mechanisms for the generation of the grating lobes in terms of the propagation of the leaky mode is given in [36, 43].

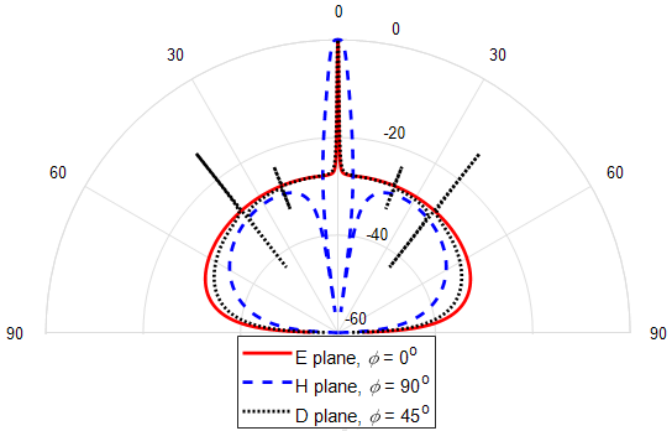

Fig. 6. Normalized radiation patterns in the E plane (ϕ = 0º), H plane (ϕ = 90º) and D plane (ϕ = 45º) for L = 0.25 cm.

An important point is that for a practical truncated structure (studied later) this grating lobe problem is largely diminished. Such narrow beams require a large radiating aperture to be formed, and thus they are found for an infinite structure. A practical finite structure, however, will largely suppress the formation of such narrow grating beams. This will be seen later in the measurement results.

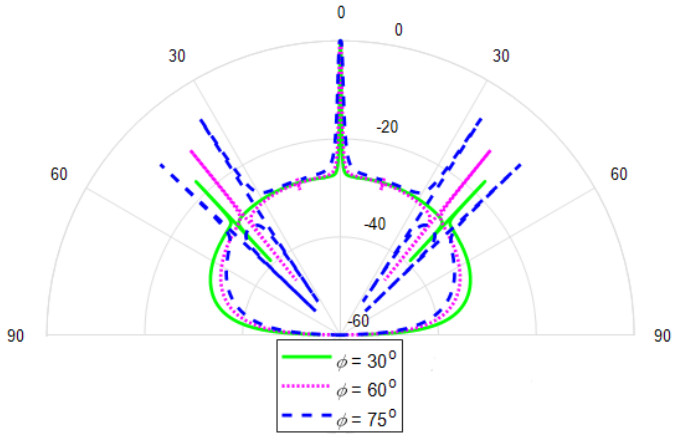

Fig. 7. Normalized radiation patterns in the ϕ = 30º plane, ϕ = 60º plane and ϕ = 75º plane for L = 0.25 cm.

In the case presented in Figs. 8 and 9, the length of the patch is a bit larger, L = 0.30 cm, the width is $W = L/5$, and the dimensions of the unit cell are given by a = 2.273 cm and $b = a/1.2$. In this case the enhancement factor is less, 70.02. Comparing Figs. 6 and 8, it is seen that the larger patches have resulted in a wider beam in both planes, although the ratio of beamwidth in the E and H planes is still roughly a factor of 10, for the same reason as before. The larger patches create more of a perturbation for the TM_0 surface wave, and hence cause the corresponding leaky mode to radiate more and have a larger attenuation constant. Conversely, smaller patches create a narrower beam. For an infinite structure, there is no limit to how narrow the beam can be made, at least for a lossless structure. (For a lossy structure, the minimum value of the attenuation constant would be that of the TM_0 surface wave mode on a lossy grounded slab without patches.) Figure 9 shows the occurrence of grating lobes just as in Fig. 7, with the grating lobes appearing in about the same directions as before, but with wider beams compared to Fig. 7 due to the increased attenuation constant of the leaky mode.

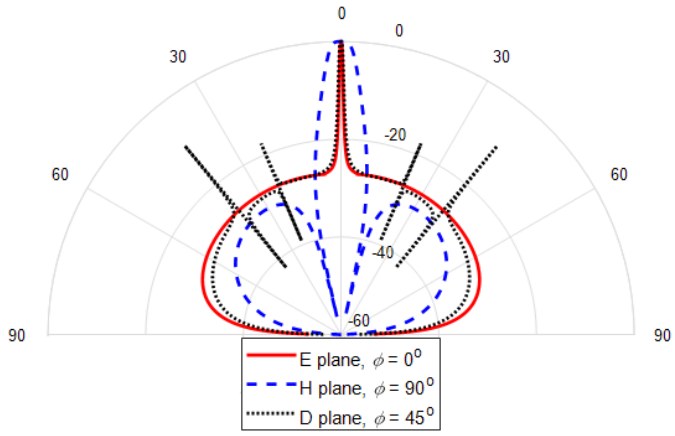

Fig. 8. Normalized radiation Patterns in the E plane (ϕ = 0º), H plane (ϕ = 90º) and D plane (ϕ = 45º) for L = 0.30 cm.

This article has been accepted for publication in a future issue of this journal, but has not been fully edited. Content may change prior to final publication. Citation information: DOI 10.1109/TAP.2019.2902639, IEEE Transactions on Antennas and Propagation

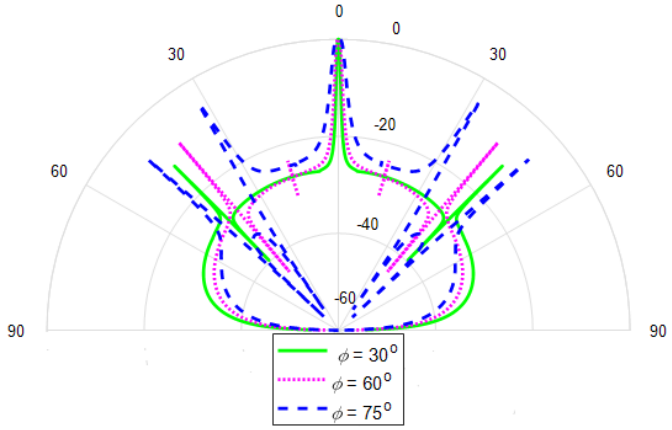

Fig. 9. Normalized radiation Patterns in the ϕ = 30° plane, ϕ = 60° plane and ϕ = 75° plane for L = 0.30 cm.

V. Variation of Main Beam with Frequency

At first the design is optimized so that the power density at broadside is maximum. Once again, the substrate is chosen to have a relative permittivity of ε_r = 9.8 and a loss tangent of tanδ = 0.002. The substrate height is h = 1.27 mm, with the excitation provided by a magnetic dipole on the ground plane. The length of the patches is L = 0.30 cm, the width is $W = L/5$, and the dimensions of the unit cell are a = 2.2728 cm and $b = a/1.2$, the same as for one of the cases in section IV (Figs. 8 and 9). The frequency is varied 0.5 GHz above and below the optimum 12 GHz to see the effects on the radiation pattern in the E plane and H plane, which are shown in Figs. 10 and 11, respectively.

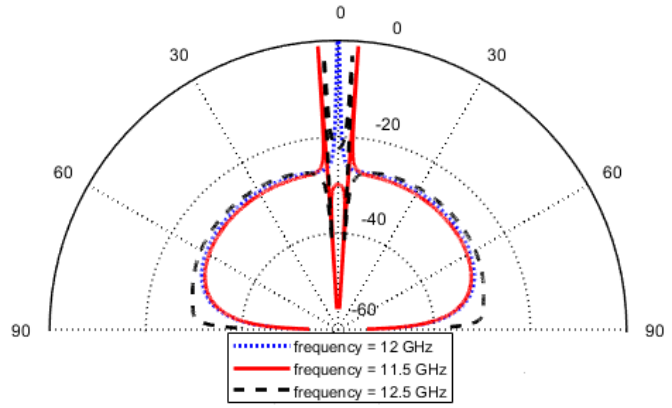

Fig. 10. Splitting of the beam in the E-plane, when the frequency is changed from the optimum frequency of 12 GHz.

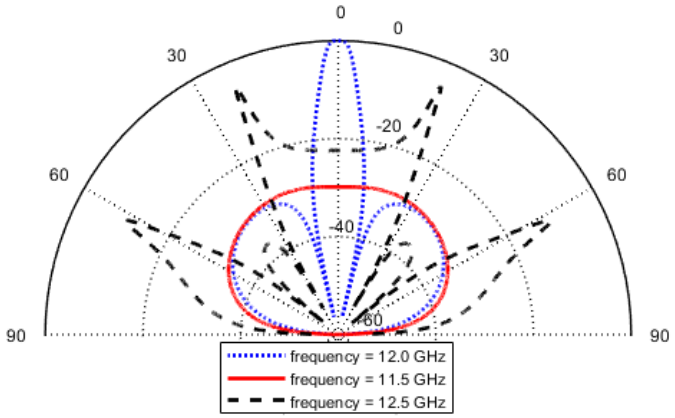

Fig. 11. Variation of the beam in the H-plane, when the frequency is changed from the optimum frequency of 12 GHz.

From Fig. 10 we see that for both increased and decreased frequency away from the optimum frequency, the main beam changes into a conical beam in the E plane. In the H plane, as seen in Fig. 11, when the frequency is varied from the optimum frequency the beam changes to a conical beam for the higher frequency but disappears for the lower frequency, leaving only a broad space-wave type of pattern. The changing of the pencil beam to a conical beam as the frequency is raised in similar to the corresponding effect seen for Fabry-Pérot resonant cavity type of leaky-wave antennas [12]. However, for a Fabry-Pérot resonant cavity type of leaky-wave antenna, the beam does not change to a conical beam as the frequency is lowered, but rather the broadside beam simply broadens. In this regard the beam behavior for the 2D periodic LWA is more similar to that observed in 1D bidirectional periodic LWAs, where the beam changes from a broadside beam to a split beam as the frequency is either raised or lowered from the optimum broadside frequency of 12 GHz [44]. The interesting exception is when the frequency is lowered in the H plane, as seen in Fig. 11. Evidently, the leaky mode in the H plane does not remain sufficiently dominant when the frequency is lowered, and the conical beam gets washed out by the residual space-wave field that is always present.

VI. CAD Formula for the Leaky-Wave Radiation Pattern

For the calculation of the pattern due to a 2D leaky wave propagating in a radial direction, the CAD formula for a bi-directional 1D leaky-wave antenna based on the complex wavenumber of the leaky mode [45] works very well, as will be demonstrated shortly. At first this might seem a bit surprising, since in the 2D case there is a radial geometric decay of $1/\rho^{1/2}$ for the leaky wave, in addition to the exponential decay from the attenuation constant. However, this is evidently compensated by the fact that as the radial distance ρ from the source on the aperture increases, a larger geometric area is enclosed in a given angular region. The net result is that the 1D formula works surprisingly well. Therefore, the CAD formula used to calculate the pattern due to the 2D radial leaky wave in either the E or H plane of the 2D periodic leaky-wave antenna is taken to be the same as that

This article has been accepted for publication in a future issue of this journal, but has not been fully edited. Content may change prior to final publication. Citation information: DOI 10.1109/TAP.2019.2902639, IEEE Transactions on Antennas and Propagation

for a bidirectional 1D leaky-wave antenna, as given in [45]. For convenience, this formula, which applies for an infinite 1D bidirectional LWA, is reproduced here (and expressed in terms of cylindrical wavenumber notation) as

$$R(\theta) = \frac{1}{k_\rho^2 - k_0^2 \sin^2\theta}\,. \tag{29}$$

(The formula can also be extended to that of a finite-size LWA [45].) The wavenumber $k_\rho = \beta - j\alpha$ is the complex wavenumber of the relevant space harmonic for the leaky mode producing either the E plane or the H plane pattern; that is, the (−1,0) or the (0,−1) harmonic, respectively. Of course, as noted before, the attenuation constant α is different for the leaky mode in the E plane and the H plane, and this is why the beamwidths are very different in these two planes. The pattern function $R(\theta)$ is derived based on the space-factor of the aperture distribution of a 1D LWA only, and ignores the element factor and polarization effects. However, in the E plane, the pattern function $R(\theta)$ denotes E_θ, while in the H plane it denotes E_ϕ for the structure and dipole excitation considered here.

A comparison of the radiation patterns from reciprocity and the CAD formula in the E plane is shown in Fig. 12 and for the H plane in Fig. 13. In the following case the length of the patches is L = 0.300 cm, the width is $W = L/5$, and the dimensions of the unit cell are given by a = 2.27271 cm and $b = a/1.2$. The substrate is taken to be lossless. The wavenumbers of the radiating (−1,0) harmonic of the leaky mode along the x-axis (E plane), and the (0,−1) harmonic of the leaky mode along the y axis (H plane) are, respectively

$$k_\rho^E / k_0 = -6.040\times10^{-4} - j\left(5.765\times10^{-4}\right),$$
$$k_\rho^H / k_0 = 0.0100 - j\left(0.0105\right),$$

where k_0 is the free space wavenumber at 12 GHz. The method used for calculating the wavenumber of the radiating leaky mode is given in section II of [36]. The total radiation pattern of the 2D periodic LWA has two components. One is due to the radiation from the leaky mode supported by the structure, and this produces the main beam at broadside. This component is approximately described by the CAD formula. The rest of the radiation pattern is due to the space wave, which is direct radiation from the source dipole. There appears to be good agreement between the main beam of the exact pattern obtained from reciprocity and that predicted by the CAD formula, as seen in Figs. 12 and 13, since the level of the space wave is fairly small (less than −30 dB relative to the peak of the main beam).

The CAD formula can also be used to calculate the main beam pattern shape, and even the location and shape of the grating lobes, in planes that are off the principal planes. However, one must then be careful in how one applies formula (29), because the radial leaky mode that is propagating at an angle $\phi = \phi_{00}$ is no longer responsible for the pattern in the plane $\phi = \phi_{00}$, but rather in the plane $\phi = \phi_{pq}$, where (p, q) is the Floquet wave that is radiating for the leaky mode propagating in the direction $\phi = \phi_{00}$. More details on this aspect may be found in [36].

Another approach for calculating the far-field radiation pattern of a 2-D periodic LWA structure of either finite or infinite size that is excited by a source was discussed in [46]. This approach was based on calculating the currents on all of the patches by using an approximate radially-propagating surface-wave formula, and then using an array factor to calculate the pattern.

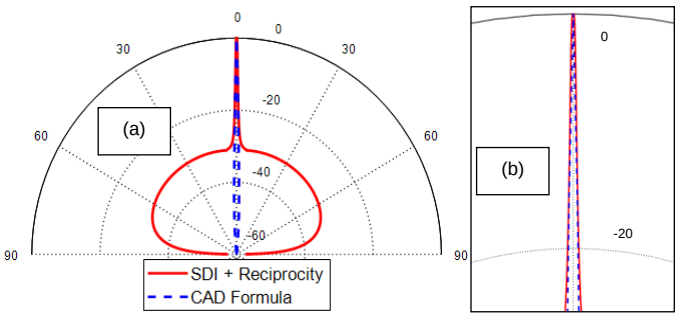

Fig. 12. (a) Pattern predicted by the CAD formula compared to the exact pattern from reciprocity in the E plane. (b) An expanded view of the main beam around the −20 dB power level.

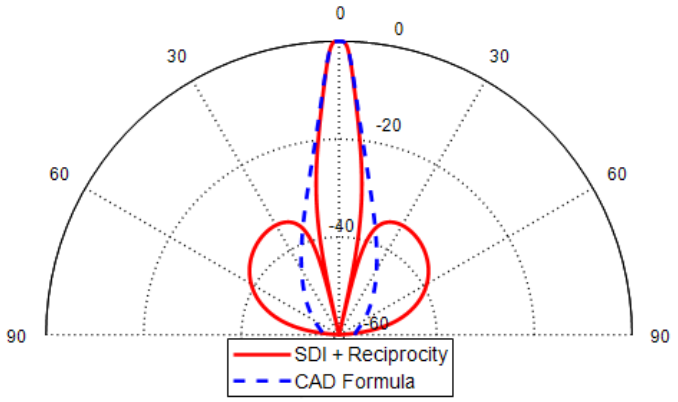

Fig. 13. Pattern predicted by the CAD formula compared to the exact pattern from reciprocity in the H plane.

VII. Cross-Section of the Beam at Different Power Levels

As noted in the previous section, the E and H plane patterns of the structure are well predicted by the leaky-wave CAD formula, and the patterns in these principal planes are smooth, without grating lobes. However, it is seen that the presence of grating lobes close to broadside affects the shape of the main beam for this structure, and this effect is examined here. Looking at a cross-section of the main beam reveals the shape of the main beam for all ϕ angles, something that is not discernible from only looking at the principal planes.

The cross-section of the beam at a power level of −3 dB is shown in Fig. 14, while Fig. 15 shows the beam cross-section at a power level of −9 dB. The frequency here is again 12 GHz. The substrate is chosen to have a relative permittivity of $\varepsilon_r = 9.8$, a loss tangent of $\tan\delta$ = 0, and the height of the substrate is h = 1.27 mm. The length of the patches is L = 0.250 cm, the width is $W = L/5$, and the dimensions of the unit cell are given by a = 2.289 cm and b = 1.224 cm.

This article has been accepted for publication in a future issue of this journal, but has not been fully edited. Content may change prior to final publication. Citation information: DOI 10.1109/TAP.2019.2902639, IEEE Transactions on Antennas and Propagation

We see from Figs. 14 and 15 that the main beam is elliptical as expected, with a beamwidth in the E plane that is about 10 times narrower than in the H plane. However, in addition, there are "spikes" extending out of the beam cross-section around $\phi \approx 85^{o}$; this effect is due to the grating lobes in the pattern. These particular grating lobes are due to the (0,−1) space harmonics of the leaky mode that propagates slightly off from the H plane direction. Interestingly, the distortion in the shape of the main beam from these spikes would never be noticed if one only examined the principal planes.

Evidently, this beam distortion is a fundamental consequence of this type of 2D periodic LWA. However, as noted before in the discussion of the grating lobes, such sharp spikes are observed here due to the infinite structure. These very narrow spikes require a large radiating aperture to form, and will be largely suppressed in a practical finite-size aperture that is truncated at the boundary, at least for cases where the truncation corresponds to a reasonable radiation efficiency (e.g., 90%), and not an impractically high efficiency.

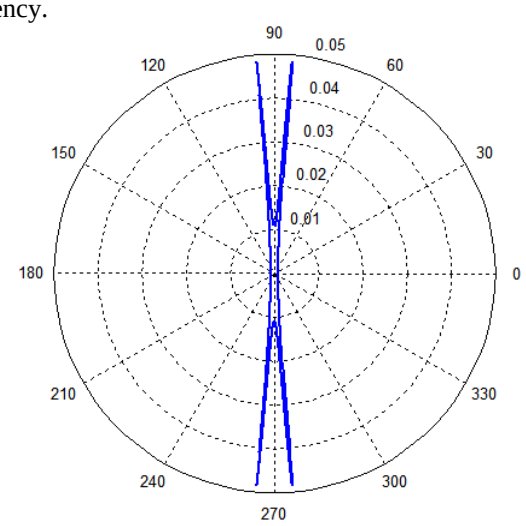

Fig. 14. Cross-section of the main beam at a power level of −3 dB.

VIII. Variation of Beamwidth and Enhancement Factor with Patch Length

The variation of the beamwidths and the enhancement factor (EF) with the dimensions of the patches is explored here. The substrate of the 2D periodic LWA here has a loss tangent of either $\tan\delta = 0.002$ (lossy case) or zero (lossless case). The length of the patches L is varied, while the width is $W = L/5$. For each different length of patch L, the length of the unit cell a is adjusted for maximum power density at broadside while maintaining the width of unit cell as $b = a/1.2$.

The variation of the beamwidths and enhancement factor with respect to length of the patches for this lossy case is given in Fig. 16, and the same plot for the lossless case ($\tan\delta = 0$) is given in Fig. 17. Note that the enhancement factor for the lossless case in Fig. 17 is plotted on a log scale.

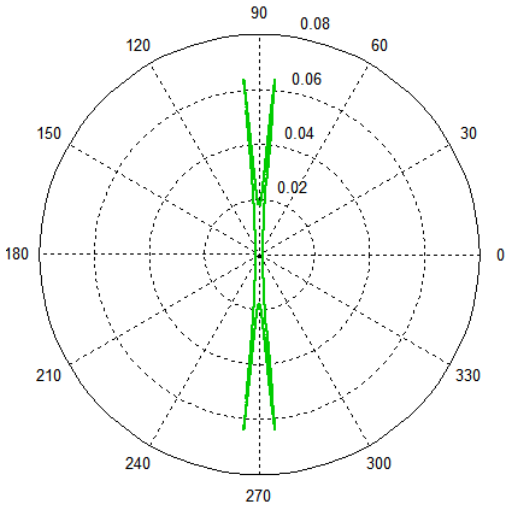

Fig. 15. Cross-section of the main beam at a power level of −9 dB.

In Fig. 16, for the lossy case, the enhancement factor and the beamwidths both decrease as the dimensions of the patches are made very small. Although the beam becomes very narrow for very small lengths of patches, the proportion of the space wave radiation relative to the leaky mode radiation increases and therefore the enhancement factor decreases. In the lossless case of Fig. 17, on the other hand, as the length of the patches becomes very small, the beamwidths decrease and the enhancement factor increases monotonically without limit.

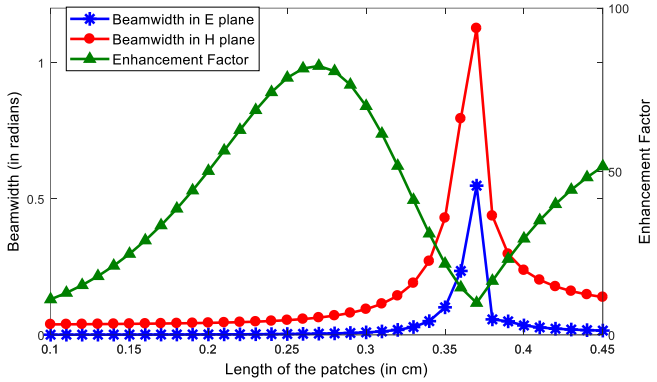

Fig. 16. Beamwidths and enhancement factor vs. length of patches for a lossy substrate.

IX. Bandwidth, Figure of Merit, and Tolerances

The bandwidth of the 2D periodic LWA for both lossy and lossless substrates is calculated here. The substrate here has a relative permittivity of $\varepsilon_r = 9.8$, and the height of substrate is $h = 1.27$ mm. The length of the patches L is varied, while the width is $W = L/5$. For each different length of patch L, the length of the unit cell a is adjusted for maximum power density at broadside while maintaining the width of unit cell as $b = a/1.2$.

This article has been accepted for publication in a future issue of this journal, but has not been fully edited. Content may change prior to final publication. Citation information: DOI 10.1109/TAP.2019.2902639, IEEE Transactions on Antennas and Propagation

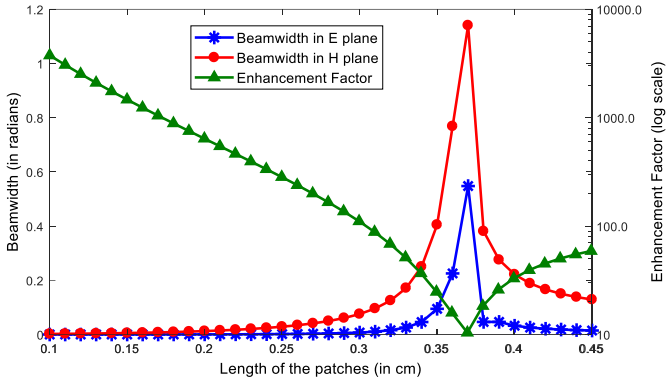

Fig. 17. Beamwidths and enhancement factor vs. length of patches for a lossless substrate.

The *figure of merit* (FoM) of the structure is defined as the fractional bandwidth times the maximum directivity of the structure. The *fractional bandwidth* (BW) is defined as the difference between the upper and lower frequencies where the power level at broadside drops by 3 dB from maximum (at the design frequency of 12 GHz where the structure is optimized), divided by the design frequency.

The *normalized tolerance* (NT) of the 2D periodic leaky-wave antenna is defined as the difference in the upper and lower values of a (length of the unit cell) at which the power level at broadside drops by 3 dB from maximum (or optimum), divided by the optimum a, expressed as a percentage. It is a measure of the degree to which the beam is sensitive to the length of the unit cell a. The exact directivity D_0 of the structure at broadside is calculated by integrating over the radiated power density, calculated using the periodic SDI and reciprocity method in Section II. The approximate directivity of a planar array is sometimes calculated from the beamwidths in the E plane and H plane using the formula [47]

$$D_0^A = \frac{\pi^2}{\Theta_E \Theta_H}, \tag{30}$$

where Θ_E is the beamwidth in the E plane and Θ_H is the beamwidth in the H plane (both in radians).

Table I lists the fractional bandwidth (BW) expressed in percent, the figure of merit (FoM), the exact (D_0) and approximate directivities (D_0^A) (absolute, not in dB), and the beamwidths in the E plane (Θ_E) and the H plane (Θ_H) for different lengths L of the patches. Here the substrate is lossless. Table I also gives the optimized a for maximum power density at broadside for each given length L of the patches.

From Table 1 we see that the approximate directivity formula, which is based on the beamwidths in the E plane and the H plane, does not work well. This is because the beam is highly asymmetric and, even more importantly, there are grating lobes in the pattern including the ones that cause the main beam distortion. These grating lobes, as well as the radiated space wave, lower the directivity. Also, it is seen that the figure of merit decreases slightly as the length of the patches is increased. For comparison, the FoM for a Fabry-Pérot resonant cavity type of antenna with a planar PRS is given by FoM = $2.48/\varepsilon_r$ [48, 49], which for this substrate material corresponds to a value of FoM= 0.253. The FoM for the 2D periodic LWA is thus about five times larger than for the Fabry-Pérot structure. However, the price that is paid is the elliptical beam shape (which may be undesirable, depending on the application) and the grating lobes. Besides causing radiation in undesired directions, the grating lobes lower the gain of the antenna. If we use D_0^A as a rough indicator of what the directivity would have been without the grating lobes, we see that the grating lobes have lowered the directivity by a factor of about 5-10, depending on the case. However, again, this is for an infinite structure, not a practical truncated structure.

TABLE I
BANDWIDTH, FIGURE OF MERIT, EXACT DIRECTIVITY, APPROXIMATE DIRECTIVITY, AND BEAMWIDTHS FOR DIFFERENT PATCH LENGTHS.

(cm)	BW (%)	D_0	FoM	Θ_E (rad)	Θ_H (rad)	D_0^A
L = 0.25 a = 2.297	0.014	11297.0	1.54	0.00168	0.0288	203823
L = 0.30 a = 2.273	0.085	1672.9	1.423	0.00729	0.0756	17918
L = 0.40 a = 2.418	0.54	221.87	1.19	0.0325	0.222	1371.2

Table II lists the fractional bandwidth (BW) in percent, the normalized tolerance (NT) in percent, and the beamwidths in the E plane (Θ_E) and the H plane (Θ_H) for a lossy substrate with loss tangent tanδ = 0.002, for different lengths L of the patches. Table II also gives the optimized a value for maximum power density at broadside for each given length L of the patches.

TABLE II
BANDWIDTH, NORMALIZED TOLERANCE, AND BEAMWIDTHS FOR DIFFERENT PATCH LENGTHS, FOR A LOSSY SUBSTRATE.

L (cm)	a (cm)	BW (%)	NT (%)	Θ_E (rad)	Θ_H (rad)
0.25	2.2971	0.049333	0.06554	0.003196	0.05404
0.30	2.2728	0.13592	0.19613	0.0092	0.0944
0.40	2.4176	0.60583	0.88194	0.03466	0.2376

From Table II we observe that the normalized tolerance of the 2D periodic leaky-wave antenna is quite low but increases when the beam is broader (which usually occurs when the size of the patches is larger). From Tables I and II we see that the bandwidth increases with the length of the patches and is larger for the lossy substrate, compared to the lossless substrate with the same length of patches, especially for smaller patches.

It is difficult to accurately determine the radiation efficiency of such a structure due to loss, either by calculation or by measurements. However, some rough estimates have been obtained. The dielectric loss and the ground plane loss can be estimated by ignoring the patches and examining the TM_0

This article has been accepted for publication in a future issue of this journal, but has not been fully edited. Content may change prior to final publication. Citation information: DOI 10.1109/TAP.2019.2902639, IEEE Transactions on Antennas and Propagation

surface wave propagation on a lossy grounded slab. The patch loss can be estimated by using a surface impedance for the patches. More details may be found in [36]. These estimates indicate that the radiation efficiency varies from about 40% to 90% as the patch length varies from 0.25 cm to 0.35 cm. larger patches mean that more of the power from the source is going to radiation as opposed to material loss, but larger patches also result in a lower directivity.

X. Measured Radiation Pattern for a Finite-Sized Structure

The theoretical analysis for the radiation patterns using the periodic spectral domain immittance method given in section II assumes an infinite structure in which the array of rectangular patches, and the substrate as well as the ground plane, extend to infinity in the *xy*-plane. However, for a practical design of a 2D periodic LWA, the infinite structure is truncated at a point where the patch currents of the leaky mode reduce sufficiently from that at the point of excitation in the center of the structure. If the distance from the E-plane edge of the structure to the central feed is d, then we should require $\exp(-2\alpha d) = p$, where α is the attenuation constant of the leaky mode in the E-plane direction, which can be found using the method in section IIIC of [36], and p is a number chosen to be sufficiently small. (The E-plane direction is used here because the leaky mode attenuates much less rapidly in this direction.) For many 1D LWAs, p is chosen as 0.1, meaning that 10% of the power in the leaky mode is left at the truncation. However, it should be noted that the truncation effects will be more serious for a 1D LWA that is designed to radiate a beam at some angle $\theta = \theta_0$ compared to a 2D LWA that radiates a beam at broadside. This is because a reflected leaky mode on a 1D LWA will result in a backward beam pointing at angle $\theta = -\theta_0$, while for the 2D LWA the reflected beam will still radiate at broadside.

For a practical 2D periodic LWA, a design has been optimized for the frequency f = 24 GHz so that the power density at broadside is maximum. The dielectric substrate is chosen to be Rogers RO4350B, having a relative permittivity of ε_r = 3.66 and a loss tangent of tan δ = 0.004 with a copper cladding thickness of 17 μm. The dielectric substrate is grounded with a copper layer and has a height h = 0.762 mm. The excitation of the antenna is provided by a narrow y-directed slot in the ground plane. The slot is centered at the location ($x_0 = -a/2$, $y_0 = 0$). Here the length of each copper patch is L = 0.31 cm, the width is $W = L/5$, and the dimensions of the unit cell are a = 1.144 cm and $b = a/1.2$. The size of the substrate board is 30.5 cm (12 inches) along the x-direction (E plane), and 22.9 cm (9 inches) along the y-direction (H plane), and can fit 27 patches along x and 23 patches along y. With this particular design, at the frequency of 24 GHz, the leaky-wave attenuation constant from theory is α = 7.37 m^{-1}. Therefore in the E plane direction, at the edge of the board (x = 15.25 cm) there is 10.6% of the power left in the leaky mode. Similarly, in the H plane direction, the leaky wave α = 54.47 m^{-1}, and at the edge of the board (y = 11.45 cm) there is 3.8×10^{-4} % of the power left in the leaky mode.

We have done two numerical analyses for the finite structure. The first one uses the method of moments (implemented in Ansys Designer) assuming an infinite ground plane and substrate (with the finite-size patch array), with the excitation provided by a small loop of current close to the ground plane. The second one uses the finite element method (implemented in Ansys HFSS) that models the actual finite structure. According to full-wave simulations, considering the finite substrate size and the loss in the dielectric and copper materials, we observed that the maximum broadside gain appears at 23.5 GHz and is 18.7 dB, and the 3dB gain bandwidth (defined as the frequency span over which the gain is maintained within 3 dB of its maximum at 23.5 GHz) is 450 MHz (1.91%).

The proposed 2D LWA is fabricated using conventional printed circuit board (PCB) techniques as shown in Fig. 18(a), and the slot on the ground plane is connected to a rectangular WR-42 waveguide, shown in Fig. 18(b). The waveguide is fed by a coaxial cable as shown in Fig. 18(b). The measurement setup consists of a transmitting antenna made of an open-ended waveguide (without flange) with a broadside gain of 6.5 dBi operating at K-band connected to a Vector Network Analyzer (VNA) using a 50 Ω coaxial cable. The transmitter is mounted on a 1 m long rotating L-shaped arm, whereas the leaky wave antenna under test is placed at the center of the rotation. The pyramidal microwave absorbers shown in Fig. 18(a) are placed under the antenna and other flat absorbers are placed on the rotating arm. The 2D LWA is used in receive mode and is connected to the VNA via a 50 Ω coaxial cable, where the measured radiation patterns are extracted from the recorded scattering parameters.

The measured radiation patterns in the E and H planes are given in Figs. 19 and 20 along with the radiation patterns obtained from the theoretical method in section II, together with results from a method of moments simulation (Ansys Designer) and a finite element method simulation (Ansys HFSS). There is very good agreement between the measured radiation patterns and the theoretical and simulated ones, especially for the main lobe at broadside. The measured maximum gain at broadside is obtained by using a calibration via a standard gain horn (G_{SGH} = 10 dB) antenna in place of the 2D periodic LWA. Since the input reflection coefficient of the LWA is below −10dB ($|S_{11}| = -12.5$ dB at 23.5 GHz), the actual gain of the leaky wave antenna is estimated via

$$G_{LWA} = G_{SGH} + 20\log\left|S_{21}^{LWA} / S_{21}^{SGH}\right|. \qquad (31)$$

Here $S_{21}{}^{LWA}$ and $S_{21}{}^{SGH}$ are the transmission coefficients when the LWA or the standard gain horn antenna is used as the receiver, respectively. This leads to a measured gain of the LWA of 17.8 dB at 23.5 GHz. The theoretical directivity of the infinite structure is 20.5 dB and the simulated gain of the truncated antenna from HFSS is 18.7 dB.

This article has been accepted for publication in a future issue of this journal, but has not been fully edited. Content may change prior to final publication. Citation information: DOI 10.1109/TAP.2019.2902639, IEEE Transactions on Antennas and Propagation

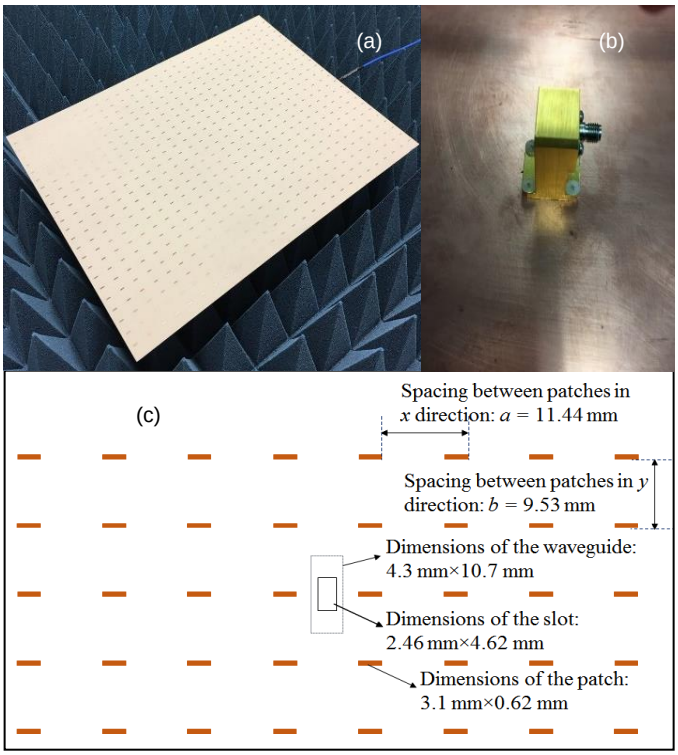

Fig. 18. The fabricated 2D periodic leaky-wave antenna. (a) Upper surface showing the array of 27×23 copper patches over a grounded dielectric layer; (b) Coaxial to rectangular waveguide adaptor attached to the bottom part of the ground plane, where a rectangular slot is used to feed the antenna; (c) Top schematic view of the 2D periodic LWA showing the metallic patches on top of the substrate along with the slot on the ground plane and the waveguide feed.

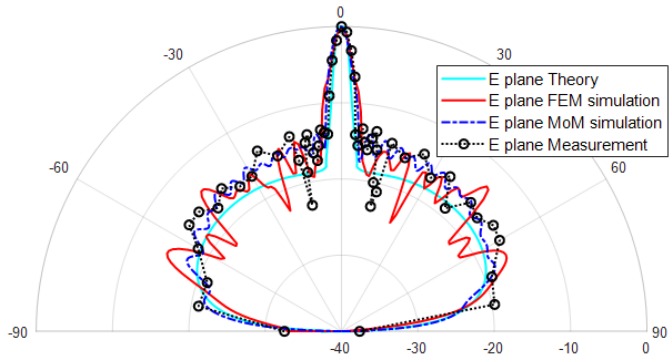

Fig. 19. Normalized radiation pattern in the E plane from measurement, theoretical calculation, and simulations in Ansys Designer (MoM) and Ansys HFSS (FEM) .

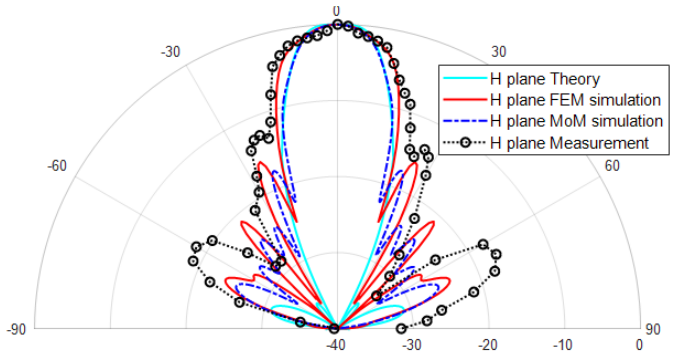

Fig. 20. Normalized radiation pattern in the H plane from measurement, theoretical calculation, and simulations in Ansys Designer (MoM) and Ansys HFSS (FEM).

XI. Conclusion

The radiation properties of a 2D periodic leaky wave antenna (one that radiated from higher-order space harmonics) has been studied in depth here for the first time, and ways to optimize and design the structure were given. The structure produces a narrow beam at broadside with a high directivity and can find application in the microwave and millimeter-wave regimes due to the extreme simplicity of the structure, consisting of only a periodic array of metal patches on a grounded slab, excited by a simple slot source. The structure is also very low profile (with a thickness of 1.27 mm for the substrate chosen here, for an operating frequency of 12 GHz). In this structure the period a in the E plane dimensions is the parameter that is adjusted to obtain maximum power radiation at broadside. The size of the patches (primarily the length) is adjusted to obtain the desired beamwidth.

The radiation characteristics of the antenna were examined using a combination of reciprocity, method of moments, and the periodic spectral domain immittance method. A simple closed-form CAD formula was also shown to be very effective at predicting the shape of the main beam and the beamwidths in the E and H planes.

One of the main characteristics of this antenna is that the main beam at broadside is highly elliptical, with the E plane beamwidth being about 10 times smaller than the H plane beamwidth, due to the fundamental differences in the attenuation constants of the leaky mode in the E and H plane directions. Another main characteristic is the appearance of grating lobes off of the principal planes, which lowers the directivity and distorts the shape of the main beam. However, these grating lobe affects appear to be mitigated somewhat for a practical truncated structure with a finite aperture size. The figure of merit (FoM) for this structure is actually higher than that obtained for a Fabry-Pérot resonant cavity type of 2D leaky-wave antenna (which does not radiate from higher-order space harmonics).

A practical 2D periodic LWA has been fabricated and measured, where the radiation patterns have been found to have excellent agreement with the theoretically calculated patterns and the simulated radiation patterns obtained by commercial software.

REFERENCES

[1] Radiating Electromagnetic Waveguide, W. W. Hansen. (1940). *U.S. Patent No. 2,402,622*.

[2] L. O. Goldstone and A. A. Oliner, "Leaky-wave antennas—Part I: Rectangular waveguides," *IRE Transactions on Antennas and Propagation*, vol. AP-7, pp. 307–319, Oct. 1959.

[3] J. N. Hines and J. R. Upson, "A wide aperture tapered-depth scanning antenna," Ohio State Univ. Res. Found., Report 667-7, Columbus, Ohio, Dec. 1957.

[4] W. Rotman and A. A. Oliner, "Asymmetrical trough waveguide antenna," *IRE Transactions on Antennas and Propagation*, vol. AP-7, pp. 153-162, Apr.1959.

[5] A. A. Oliner, "Scannable millimeter wave arrays," Final Report on RADC Contract No. F19628-84-K-0025, Polytechnic University, Sep. 30, 1988, (two volumes).

[6] G. V. Trentini, "Partially reflecting sheet arrays," *IEEE Transactions on Antennas and Propagation*, vol. 4, pp. 666-671, Oct. 1956.

[7] N. G. Alexopoulos and D. R. Jackson, "Fundamental superstrate (cover) effects on printed circuit antennas," *IEEE Transactions on Antennas and Propagation*, vol. 32, pp. 807- 816, Aug. 1984.

[8] D. R. Jackson and N. G. Alexopoulos, "Gain enhancement methods for printed circuit antennas," *IEEE Transactions on Antennas and Propagation*, vol. 33, pp. 976-987, Sep. 1985.

[9] D. R. Jackson and A. A. Oliner, "A leaky-wave analysis of the high-gain printed antenna configuration," *IEEE Transactions on Antennas and Propagation*, vol. 36, pp. 905-910, Jul. 1988.

[10] D. R. Jackson, A. A. Oliner, and A. Ip, "Leaky-wave propagation and radiation for a narrow-beam multiple-layer dielectric structure," *IEEE Transactions on Antennas and Propagation*, vol. 41, pp. 344-348, Mar. 1993.

[11] P. Feresidis and J. C. Vardaxoglou, "High gain planar antenna using optimised partially reflective surfaces," *IEE Proceedings on Microwaves Antennas and Propagation*, vol. 148, pp. 345-350, Dec. 2001.

[12] T. Zhao, D. R. Jackson, J. T. Williams, H. Y. Yang, and A. A. Oliner, "2-D periodic leaky-wave antennas -- Part I: Metal patch design," *IEEE Transactions on Antennas and Propagation*, vol. 53, pp. 3505-3514, Nov. 2005.

[13] G. Lovat, P. Burghignoli, F. Capolino, D. R. Jackson, and D. R. Wilton, "Analysis of directive radiation from a line source in a metamaterial slab with low permittivity," *IEEE Transactions on Antennas and Propagation*, vol. 54, no. 3, pp. 1017–1030, Mar. 2006.

[14] G. Lovat, P. Burghignoli, F. Capolino, and D. R. Jackson, "On the combinations of low/high permittivity and/or permeability substrates for highly directive planar metamaterial antennas," *IET Microwaves, Antennas and Propagation*, vol. 1, no. 1, pp. 177–183, Feb. 2007.

[15] J. R. Kelly and A. P. Feresidis, "Array antenna with increased element separation based on a Fabry–Pérot resonant cavity with AMC walls," *IEEE Transactions on Antennas and Propagation*, vol. 57, no. 3, pp. 682–687, Mar. 2009.

[16] Y. Sun, Z. N. Chen, Y. Zhang, H. Chen, and T. S. P. See, "Subwavelength substrate-integrated Fabry-Pérot cavity antennas using artificial magnetic conductor," *IEEE Transactions on Antennas and Propagation*, vol. 60, no. 1, pp. 30–35, Jan. 2012.

[17] J. Liu, D. R. Jackson, Y. Long, "Substrate integrated waveguide (SIW) leaky-wave antenna with transverse slots," *IEEE Transactions on Antennas and Propagation*, vol. 60, no. 1, pp. 20-29, Jan. 2012.

[18] F. Xu, K. Wu, X. Zhang, "Periodic leaky-wave antenna for millimeter wave applications based on substrate integrated waveguide," *IEEE Transactions on Antennas and Propagation*, vol. 58, no. 2, pp. 340-347, Feb. 2010.

[19] M. Guglielmi, D. R. Jackson, "Broadside radiation from periodic leaky-wave antennas," *IEEE Transactions on Antennas and Propagation*, vol. 41, no. 1, pp. 31-37, Jan. 1993.

[20] Y. Kaganovsky, R. Shavit, "Full wave analysis of electric and magnetic line sources in the presence of a strip grating over a grounded dielectric slab structure," *The Second European Conference on Antennas and Propagation (EuCAP)*, pp. 1-5, 11-16 Nov. 2007, Edinburgh, Scotland, UK.

[21] S. Otto, A. Rennings, K. Solbach, C. Caloz, "Transmission line modeling and asymptotic formulas for periodic leaky-wave antennas scanning through broadside," *IEEE Transactions on Antennas and Propagation*, vol. 59, no. 10, pp. 3695-3709, Oct. 2011.

[22] W. A. Johnson, S. Paulotto, D. R. Jackson, D. R. Wilton, W. L. Langston, L. I. Basilio, P. Baccarelli, G. Valerio, F. T. Celepcikay, "Modeling of general 1-D periodic leaky-wave antennas in layered media using EIGER™," *International Conference on Electromagnetics in Advanced Applications (ICEAA)*, pp. 205-208, 20-24 Sep. 2010, Sydney, Australia.

[23] S. K. Podilchak, S. F. Mahmoud, A. l. P. Freundorfer, Y. M. M. Antar, "Perturbation analysis of planar periodic leaky-wave antennas fed by cylindrical surface-waves," *URSI General Assembly and Scientific Symposium*, pp. 1-4, 13-20 Aug. 2011, Istanbul. Turkey.

[24] C. Caloz and T. Itoh, "Array factor approach of leaky-wave antennas and application to 1-D/2-D composite right/left-handed (CRLH) structures," *IEEE Microwave and Wireless Components Letters*, vol. 14, no. 6, pp. 274-276, Jun. 2004.

[25] P. Baccarelli, P. Burghignoli, G. Lovat, S. Paulotto, "A novel printed leaky-wave 'bull-eye' antenna with suppressed surface-wave excitation", *(2004) IEEE Antennas and Propagation Society, AP-S International Symposium (Digest)*, vol. 1, pp. 1078-1081, Jun. 2004.

[26] A. Foroozesh, R. Paknys, D. R. Jackson, J. J. Laurin, "Beam focusing using backward-radiating waves on conformal leaky-wave antennas based on a metal strip grating," *IEEE Transactions on Antennas and Propagation*, vol. 63, no. 11, pp. 4667-4677, Nov. 2015.

[27] A. Foroozesh, L. Shafai, "2-D truncated periodic leaky-wave antennas with reactive impedance surface ground planes," *IEEE Antennas and Propagation Society Intl. Symp.*, 9-14 July 2006, Albuquerque, NM.

[28] M. Lorente-Crespo, C. Mateo-Segura, "Analysis of 2-D periodic leaky-wave nano-antennas in the NIR," *IEEE Antennas and Propagation Society Intl. Symp.*, 6-11 Jul. 2014, Charleston, SC.

[29] C. Mateo-Segura, G. Goussetis, A. P. Feresidis, "Analysis of 2-D periodic leaky wave antennas with subwavelength profile," *IEEE Antennas and Propagation Society Intl. Symp.*, 1-5 Jun. 2009, Charleston, SC.

[30] J. R. Kelly, T. Kokkinos, A. P. Feresidis, "Analysis and design of sub-wavelength resonant cavity type 2-D leaky-wave antennas," *IEEE Transactions on Antennas and Propagation*, vol. 56, no. 9, pp. 2817-2825, Sep. 2008.

[31] C. Mateo-Segura, M. Garcia-Vigueras, G. Goussetis, A. P. Feresidis, J. L. Gomez-Tornero, "A simple technique for the dispersion analysis of Fabry-Perot cavity leaky-wave antennas," *IEEE Transactions on Antennas and Propagation*, vol. 60, no. 2, pp. 803-810, Feb. 2012.

[32] T. W. Ebbesen, H. J. Lezec, T. F. Ghaemi, T. A. Thio, P. A. Wolf, "Extraordinary optical transmission through subwavelength hole arrays," *Nature*, vol. 391, pp 667-669, Feb. 1998.

[33] H. J. Lezec, A. Degiron, E. Devaux, R. A. Linke, L. Martin-Moreno, F. J. Garcia-Vidal, T. W. Ebbesen, "Beaming Light from a Subwavelength Aperture," *Science*, vol. 297, issue 5582, pp. 820-822, Aug. 2002.

[34] D. R. Jackson, A. A. Oliner, T. Zhao, and J. T. Williams, "Beaming of light at broadside through a subwavelength hole: Leaky wave model and open stopband effect," *Radio Science*, vol. 40, Sep. 2005.

[35] D. R. Jackson, J. Chen, R. Qiang, F. Capolino, and A. A. Oliner, "The role of leaky plasmon waves in the directive beaming of light through a subwavelength aperture," *Optics Express*, vol. 16, no. 26, 22 Dec. 2008.

[36] S. Sengupta, D. R. Jackson, S.A. Long, "Modal analysis and propagation characteristics of leaky waves on a 2D periodic leaky-wave antenna," *IEEE Transactions on Microwave Theory and Techniques*, vol. 66, no. 3, pp. 1181-1191, Mar. 2018.

[37] S. Sengupta, D. R. Jackson, S.A. Long, "Propagation characteristics of leaky waves on a 2D periodic leaky-wave antenna," *IEEE MTT-S International Microwave Symposium*, 4-9 Jun. 2017.

[38] S. Sengupta, D. R. Jackson, S.A. Long, "Properties of Microwave and Optical 2-D Periodic Leaky Wave Antennas," *2015 Texas Symposium on Wireless and Microwave Circuits and Systems (WMCS)*, 23-24 Apr. 2015, Waco, TX.

[39] S. Sengupta, D. R. Jackson, S.A. Long, "Examination of radiation from 2D periodic leaky-wave antennas," *2014 USNC-URSI Radio Science Meeting (Joint with AP-S Symposium)*, 6-11 Jul. 2014, Memphis, TN.

[40] K. A. Michalski and J. R. Mosig, "Multilayered media Green's functions in integral equation formulations," *IEEE Transactions on Antennas and Propagation*, vol. 45, no. 3, pp. 508–519, Mar., 1997.

[41] T. K. Sarkar, "A note on the choice of weighting functions in the method of moments," *IEEE Transactions on Antennas and Propagation*, vol. 33, pp. 436–4421, Apr. 1985.

[42] T. K. Sarkar, A. R. Djordjevic, and B. M. Kolundzija, "Method of moments applied to antennas," Chapter 8 of *Handbook of Antennas in Wireless Communications*, CRC Press, 2001.
[43] S. Sengupta, "Properties of a 2D periodic leaky-wave antenna at microwave and optical frequencies," Ph.D. dissertation, ECE, Univ. of Houston, Houston, TX, 2016.
[44] P. Burghignoli, G. Lovat, and D. R. Jackson, "Analysis and optimization of leaky-wave radiation at broadside from a class of 1-D periodic structures," *IEEE Transactions on Antennas and Propagation*, vol. 54, no. 9, pp. 2593–2604, Sept. 2006.
[45] C. Caloz, D. R. Jackson, and T. Itoh, "Leaky-Wave Antennas," Chapter 9 in *Frontiers in Antennas, Next Generation Design and Engineering*, Frank B. Gross (Ed.), 1st Ed., McGraw-Hill, 2011.
[46] P. Burghignoli, G. Lovat, and D. R. Jackson, "An investigation of radiation at broadside from leaky plasmon waves on periodic structures" *Intl. Conference on Electromagnetics in Advanced Applications (ICEAA)*, Sept. 12–16, 2005.
[47] C. A. Balanis, *Antenna Theory, Analysis and Design*, 3rd Ed., Wiley, New Jersey, 2005.
[48] D. R. Jackson *et al.*, "The fundamental physics of directive beaming at microwave and optical frequencies and the role of leaky waves," *Proc. IEEE*, vol. 99, no. 10, pp. 1780–1805, Oct. 2011.
[49] G. Lovat, P. Burghignoli, F. Capolino, and D. R. Jackson, "Highly-directive planar leaky-wave antennas: a comparison between metamaterial-based and conventional designs," *Proc. Eur. Microw. Assoc.*, vol. 12, p. 21, Mar. 2006.

Sohini Sengupta was born in Kolkata, West Bengal, India in 1985. Dr. Sengupta received her Bachelors degree in electronics and communication engineering from the Heritage Institute of Technology, in Kolkata, West Bengal, India, in the year 2007. She joined the University of Houston, in Houston, Texas, USA, as a student in 2009 and graduated with a MS in electrical engineering in 2012. She then obtained her PhD in electrical engineering from the same university in the year 2016.

Between 2011 and 2016 she was a Teaching Assistant at the Department of Electrical and Communication Engineering at the University of Houston, Houston, Texas. She worked as a Post-Doctoral Fellow and Lecturer at the University of Houston in Houston, Texas for a year from 2016 to 2017. Presently she is working as an Antenna Design Engineer at Energous Corporation in San Jose, California, USA since 2017. She has previously published journal papers on linear microstrip series-fed antenna array, 2D periodic leaky wave antennas and several conference papers on different areas. Her research interests include microstrip antennas, arrays, numerical methods, leaky-wave antennas, radar cross-section reduction techniques, antenna miniaturization techniques.

David R. Jackson was born in St. Louis, MO on March 28, 1957. He obtained the B.S.E.E. and M.S.E.E. degrees from the University of Missouri, Columbia, in 1979 and 1981, respectively, and the Ph.D. degree in electrical engineering from the University of California, Los Angeles, in 1985. From 1985 to 1991 he was an Assistant Professor in the Department of Electrical and Computer Engineering at the University of Houston, Houston, TX. From 1991 to 1998 he was an Associate Professor in the same department, and since 1998 he has been a Professor in this department. He has been a Fellow of the IEEE since 1999. His present research interests include microstrip antennas and circuits, leaky-wave antennas, leakage and radiation effects in microwave integrated circuits, periodic structures, and electromagnetic compatibility and interference.

He is presently serving as the chair of USNC-URSI, the U.S. National Committee (USNC) of URSI, the International Union of Radio Science. He is also on the Education Committee of the Antennas and Propagation Society (AP-S) and on the MTT-15 (Microwave Field Theory) Technical Committee of the Microwave Theory and Techniques Society.

Previously, he has been chair of the Distinguished Lecturer Committee of the IEEE Antennas and Propagation Society (AP-S), the chair of the Transnational Committee of the IEEE AP-S, the chair of the Chapter Activities Committee of the AP-S, a Distinguished Lecturer for the AP-S, a member of the AdCom for the AP-S, and an Associate Editor for the IEEE Transactions on Antennas and Propagation. He previously served as the chair of the MTT-15 (Microwave Field Theory) Technical Committee. He has also served as the chair of Commission B of USNC-URSI and as the Secretary of this Commission. He also previously served as an Associate Editor for the Journal Radio Science and the International Journal of RF and Microwave Computer-Aided Engineering.

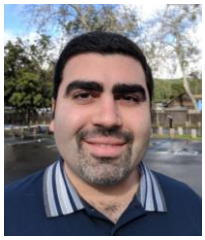

Ahmad T. Almutawa (S'05–M'06) was born in Kuwait City, Kuwait, in 1984. He received the B.S. and M.S. degree in electrical engineering from Kuwait University, Kuwait City, Kuwait, in 2006 and 2009 respectively; the M.S. degree in electrical engineering (wireless circuits and systems) from the University of South Florida, Tampa, FL, USA, in 2011. He is currently pursuing the Ph.D. degree in electrical engineering (electromagnetics and metamaterials) with the University of California, Irvine, CA, USA. Since 2011, he has been a faculty member with the Electronic Engineering Technology Department, Public Authority for Applied Education and Training, Kuwait City, Kuwait. His current research interests include leaky-wave antennas, metamaterial-based antennas.

Hamidreza Kazemi received his B.Sc. degree in electrical engineering from Isfahan University of Technology, Isfahan, Iran, in 2012, and the M.Sc. degree in electrical engineering from Sharif University of Technology, Tehran, Iran, in 2014. He is currently pursuing the Ph.D. degree in electrical engineering at the University of California, Irvine, CA, USA.
Mr. Kazemi was a recipient of the UC Irvine's Department Fellowship award in 2015 and 2016. His research interests include characterization of metamaterials and metasurfaces, space/time periodic electromagnetic structures, RF and Bio sensors, dispersion engineering, RF bandgap circuits and oscillators, leaky wave and millimeter wave antennas and numerical methods in electromagnetics.

This article has been accepted for publication in a future issue of this journal, but has not been fully edited. Content may change prior to final publication. Citation information: DOI 10.1109/TAP.2019.2902639, IEEE Transactions on Antennas and Propagation

Filippo Capolino (S'94–M'97–SM'04) received the Laurea (*cum laude*) and the Ph.D. degrees in electrical engineering from the University of Florence, Italy, in 1993 and 1997, respectively. He is currently a Professor with the Department of Electrical Engineering and Computer Science of the University of California, Irvine, CA, USA. Previously he has been an Assistant Professor with the Department of Information Engineering of the University of Siena, Italy till 2002. From 1997 to 1999, he was a Fulbright and then a Postdoctoral Fellow with the Department of Aerospace and Mechanical Engineering, Boston University, MA, USA. From 2000 to 2001, part of 2005 and in 2006, he was a Research Assistant Visiting Professor with the Department of Electrical and Computer Engineering, University of Houston, TX, USA. He has been a Visiting Professor at the Fresnel Institute, Marseille, France (2003) and at the Centre de Recherche Paul Pascal, Bordeaux, France (2010). His current research interests include metamaterials and their applications, traveling wave tubes, antennas, sensors in both microwave and optical ranges, plasmonics, microscopy, wireless systems, millimeter wave chip-integrated antennas and applied electromagnetics in general. He was the EU Coordinator of the EU Doctoral Programs on Metamaterials from 2004 to 2009.

Stuart A. Long was born in Philadelphia, Pennsylvania on March 6, 1945 and completed his secondary education in Snyder, Texas. He was granted the B.A. (magna cum laude) and M.E.E. degrees in Electrical Engineering from Rice University, Houston, Texas, in 1967 and 1968, respectively, and the Ph.D. degree in Applied Physics from Harvard University, Cambridge, Massachusetts, in 1974.

He has been a faculty member in the Department of Electrical and Computer Engineering at the University of Houston for the past 45 years. He is presently Associate Dean of Undergraduate Research and the Honors College, was Chair of the Department of Electrical and Computer Engineering from 1981-1995, was Interim Dean of the Honors College from 2008-2009, and in 2010-2011 served as Interim Vice Chancellor and Vice President for Research and Technology Transfer. In 2009 he was named as the first recipient of the University of Houston Career Teaching Excellence Award, and in 2010 he received the Esther Farfel Award, the highest faculty award given at the University of Houston. His research interests are in the broad area of applied electromagnetics and more specifically in microstrip and dielectric resonator antennas.

Dr. Long was elected President of the IEEE Antennas and Propagation Society (AP-S) in 1996. He also served on the IEEE Technical Activities Board, was TAB Magazines Chair and a member of the Periodicals Review Committee from 1997-99, was a Member-at-Large of the IEEE Publications Activities Board from 1998-2003, and served on the Spectrum Editorial Board from 2002-05. He was elected to serve on the Board of Directors of the IEEE for 2005-06 as Director of Division IV.

Dr. Long is a member of Phi Beta Kappa, Tau Beta Pi, Sigma Xi, and Commission B of URSI, was elected to membership in the Electromagnetics Academy in 1990, became a Fellow of the IEEE in 1991, served as an IEEE Antennas and Propagation Society Distinguished Lecturer from 1992-94, was awarded the IEEE Millennium Medal in 2000, received the IEEE Antennas and Propagation Society Outstanding Service Award in 2007, the AP-S John Kraus Antenna Award in 2014, and the AP-S Chen-To Tai Distinguished Educator Award in 2018.